Adjustable noiselike pulses from a figure-eight fiber laser

Olivier Pottiez,[1,*] Rubén Grajales-Coutiño,[2] Baldemar Ibarra-Escamilla,[3] Evgeny A. Kuzin,[3] and Juan Carlos Hernández-García[1]

[1]Centro de Investigaciones en Óptica, Loma del Bosque 115, Col. Lomas del Campestre, León, Gto. 37150, Mexico

[2]Escuela de Ciencias, Universidad Autónoma "Benito Juárez" de Oaxaca, Av. Universidad S/N, Ex Hacienda Cinco Señores, Oaxaca de Juárez, Oax. 68120, Mexico

[3]Instituto Nacional de Astrofísica, Óptica y Electrónica (INAOE), Departamento de Óptica, Luis Enrique Erro 1, Puebla, Pue. 72000, Mexico

*Corresponding author: pottiez@cio.mx

Received 29 March 2011; revised 18 May 2011; accepted 19 May 2011; posted 20 May 2011 (Doc. ID 144971); published 27 June 2011

We propose and study experimentally and numerically a passively mode-locked figure-eight fiber laser scheme generating noiselike optical pulses, or subns wave packets with a fine inner structure of subps pulses presenting random amplitudes and durations. The particular design of the nonlinear optical loop mirror (NOLM) used in this laser, relying on nonlinear polarization rotation, allows adjusting the switching power through input polarization control. Experimental results show stable pulsed operation over a limited range of the NOLM input polarization angle. Interestingly, the spectral and temporal characteristics of these pulses are observed to be widely variable over that range. In particular, the spectral width varies from 16 to 52 nm and this spectral variation is associated with an inverse evolution in the durations of the bunch and of the inner ultrashort pulses. Simulation results are in good agreement with the experiment. They confirm the strong dependence of the pulse properties on the value of the NOLM switching power, although NOLM switching is not alone responsible for the appearance of the noiselike pulsing mode.

OCIS codes: 060.3510, 140.3538, 140.4050, 190.4370.

1. Introduction

Passively mode-locked fiber lasers are simple, compact, and low-cost sources of ultrashort pulses that are attractive for a wide range of applications. These lasers include two main categories: the ring cavity design, in which nonlinear polarization evolution in the cavity in association with a polarizer provides the nonlinear switching mechanism [1], and the so-called figure-eight laser architecture [2], which presents the advantage that nonlinear switching is provided by a nonlinear optical loop mirror (NOLM) [3] (or alternatively of a nonlinear amplifying loop mirror[4]), and is thus decoupled from the ring laser structure, allowing increased flexibility [5].

There has been an increasing interest recently in the study of a particular regime of passively mode-locked fiber ring lasers, that of the so-called noiselike pulses [6–13], motivated by the perspective of superbroadband sources of high-energy pulses, very useful for applications like supercontinuum generation [9] and sensing [14]. The "noiselike" pulses are long waveforms with a fine inner structure of subps pulses with randomly varying amplitude and duration. Typical features of such pulses include a very large and smooth optical spectrum (usually of several tens of nm bandwidth), a double-scaled autocorrelation trace with a subps peak riding a wide subns pedestal, and low temporal coherence. Their energy can

0003-6935/11/250E24-08$15.00/0

be as high as 15 nJ [11] and is thus significantly higher than the energy of the pulses from the more conventional soliton lasers [2] and stretched-pulse lasers [15,16], and only compares to the energy of highly chirped pulses generated in the normal-dispersion regime [17].

A striking feature of the publications on noiselike pulsed operation of passively mode-locked fiber ring lasers is the lack of unanimity on the mechanisms invoked to explain the formation of these unusual pulses. In [6], pulse formation is attributed to the large and nonuniform cavity birefringence causing frequency-dependent transmission of the nonlinear element. In [10,11], the pulse collapse effect [18] is invoked. Although in most references anomalous-dispersion cavities are presented, noiselike-pulses generation was also demonstrated in all-normal-dispersion fiber ring lasers. And there again the interpretations diverge. In [13], pulse formation is related to the decomposition of isolated picosecond pulses that are unstable for certain sets of cavity parameters and in [12], the peak power clamping effect is invoked: when a pulse peak power gets clamped to the switching point of the nonlinear transmission, the remaining available gain no longer increases the pulse energy but instead amplifies the accompanying dispersive waves, whose interference with the pulse results in the observed noiselike pattern.

In several Papers, it was noticed that the properties of noiselike pulses, like their spectral width and shape, or the duration of the bunch, depend on laser parameters. For example, it was observed that changing the pump power affects the energy and width of the bunch (but without modifying the average duration of the inner pulses, nor the spectral width) [8,10], or the shape of the optical spectrum [12]. By adjusting the linear cavity phase delay, it is even possible to switch the laser between different modes including conventional single-pulse and noiselike pulse regimes [7,10–13]. Through complex birefringence manipulations of the ring cavity using polarization controllers, dual-wavelength noiselike regimes were also demonstrated [7]. Finally, it was shown in [8] that the pulses optical bandwidth strongly depends on intracavity dispersion.

In this Paper, we focus on the dependence of noiselike pulse properties on the switching power of the nonlinear transmission characteristic, for a fixed value of the linear phase bias. The device under study is a figure-eight fiber laser scheme, in which the nonlinear element is a NOLM presenting a particular design: unlike most conventional designs [3,19,20], it is imbalanced in polarization and not in power, and its switching relies on nonlinear polarization rotation [21]. As it was shown in earlier publications [22,23], one particularity of this scheme is the flexibility of the nonlinear transmission dependence obtained by controlling the polarization in the device. In the present case, the NOLM switching power is controlled through the angle of linear input polarization. We show that this adjustment allows tuning the temporal and spectral properties of the noiselike pulses. The experimental and numerical results presented here shed some light on the importance of the nonlinear switching element in the pulse formation process.

2. Experimental Setup

The experimental setup is presented in Fig. 1. This design is similar to those used in previous works for the generation of conventional (sub-)ps pulses [24–26], except that in the present case polarization is set linear instead of circular at the NOLM input. The figure-eight laser is formed by a NOLM (on the right side of the figure) inserted in a ring laser cavity (left part). The ring cavity includes a 4 m long Erbium-doped fiber (EDF) with 1000 ppm erbium concentration, which is pumped by a 980 nm laser diode through a WDM coupler. The maximum pump power that can be coupled into the fiber is estimated to be ~300 mW. The cavity also includes a polarizer (P) and a polarization controller consisting of two retarder plates, which is used to maximize the power

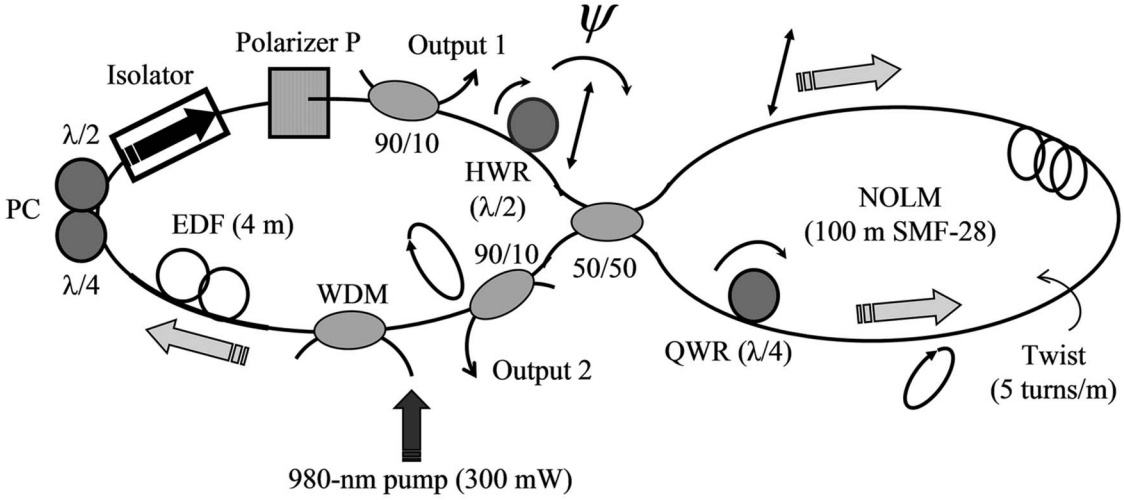

Fig. 1. Experimental setup.

transmission through the polarizer. An optical isolator ensures unidirectional laser operation. A half-wave retarder (HWR) plate controls the angle of linear polarization at the NOLM input. Two 90/10 couplers (10% output coupling) provide the laser output ports.

The NOLM is formed by a 50/50 coupler, whose output ports were fusion spliced with a $L = 100\,\mathrm{m}$ length of low-birefringence, highly twisted Corning SMF-28 fiber. The NOLM is power symmetric, and a quarter-wave retarder (QWR) is inserted in the loop, at one end of the fiber span, in order to break polarization symmetry. The clockwise beam polarization is linear, and the QWR transforms the polarization of the counterclockwise beam from linear to elliptic (the value of ellipticity depending on the relative angle between input polarization and the QWR). In spite of their equal powers, the counterpropagating beams accumulate a nonlinear phase shift difference through nonlinear polarization rotation, which provides NOLM switching [21]. A twist rate of 5 turns/m is imposed to the fiber loop, which is used to reduce the effects of residual fiber birefringence. This happens in two ways. First, twist causes a rapid precession of the fiber principal axes, so that residual birefringence tends to be averaged out. Secondly, twist induces optical activity (circular birefringence), causing light polarization to rotate along the fiber. Twist-induced polarization rotation amounts to ~5% of the twist rate, and is useful to reduce the effect of stress-induced birefringence, which typically results from bending when the fiber is wound on a spool after twisting (in this case, there is no precession of the polarization axes). Hence, for a sufficient amount of twist, the fiber behaves like an ideal isotropic fiber [27], ensuring that the ellipticity of each beam is maintained through the whole fiber span. The fiber loop has an anomalous dispersion of $\sim 17\,\mathrm{ps/nm/km}$ and a nonlinear coefficient $\gamma = 1.5\,\mathrm{W^{-1}\,km^{-1}}$ for linearly polarized light (the nonlinear coefficient for circular polarization is $\beta = 2/3\gamma = 1\,\mathrm{W^{-1}\,km^{-1}}$). With these parameters, the minimum continuous-wave switching power of the NOLM (at zero low-power transmission) is $P_{\pi\,\mathrm{min}} = 4\pi/\beta L \approx 125\,\mathrm{W}$ [22]. By controlling the angle of linear input polarization, the switching power can be adjusted continuously between this minimum and infinity, without altering the value of low-power transmission if the QWR angle is fixed [22,23].

The QWR allows precise adjustment of the NOLM low-power transmission, which should be small and yet different from zero to allow lasing to initiate [2,25]. On the other hand, the adjustment of the orientation of input polarization allows adjusting the NOLM switching power. If the QWR angle is adjusted for zero low-power transmission, then for linear input polarization forming an angle ψ with respect to the QWR axes, the NOLM transmission writes as $T = 0.5 - 0.5\cos(\pi P_{\mathrm{in}}/P_{\pi})$, where P_{in} is the NOLM input power and $P_{\pi} = P_{\pi\,\mathrm{min}}/\sin(2\psi)$ is the switching power, which can be adjusted between

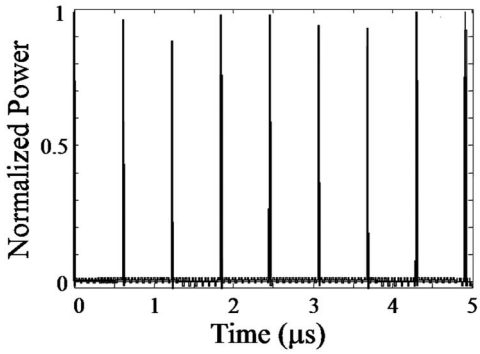

Fig. 2. Oscilloscope trace of the detected pulse train.

$P_{\pi\,\mathrm{min}}$ and infinity by adjusting the angle ψ. This mode of operation of the NOLM under linear input polarization was previously demonstrated theoretically [22] and experimentally [23]. Although these results are valid strictly speaking in the continuous-wave approximation only (case of large, ns pulses), they still apply qualitatively in the case of ultrashort pulses [28]. Finally, the same behavior is found if the QWR angle departs from zero low-power transmission.

3. Experimental Results

At maximal pump power, for proper adjustments of the HWR and QWR, a mechanical stimulation (a kick) results in mode-locking operation. Self-starting mode locking was not observed. The optical signal detected by a 2 GHz photodetector and monitored using a 500 MHz oscilloscope reveals a periodic pulse train whose repetition rate is ~1.6 MHz, indicating fundamental frequency mode locking of the ~120 m long laser cavity (Fig. 2).

The optical spectrum of the pulse train was measured using an optical spectrum analyzer (Fig. 3). A very wide and smooth spectrum is obtained, with a maximum near 1570 nm. An interesting observation is that, through adjusting the angle of the HWR inserted at the NOLM input, the 3 dB bandwidth $\Delta\lambda_{\mathrm{FWHM}}$ of the pulses can be adjusted over a wide range, from 16 to 52 nm (at Output 1). This range

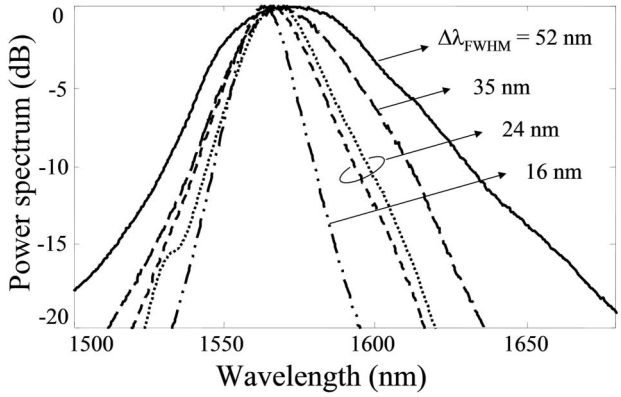

Fig. 3. Optical spectra of the mode-locked pulses measured at Output 1 (solid, dashed and dashed-dotted) and Output 2 (dotted) for different adjustments of the HWR.

corresponds to a variation of the HWR angle of about 20°. In contrast, the average power measured at Output 1 remains relatively constant (~4 mW) over that range, with ~8% variations that do not fit a systematic growth or decrease. If the HWR is rotated beyond these limits, mode locking is lost and the laser operates in the continuous-wave regime. In most cases a smooth spectrum free of narrow spectral line is observed, which confirms that the pulses are free of continuous-wave component. Even though such a narrow line sometimes appears in the mode-locked spectrum, it is quite unstable and disappears after a small adjustment of one of the retarders.

Figure 3 also shows that, as bandwidth increases, the spectrum grows faster on the long-wavelength side than on the short-wavelength side, creating in the spectrum an asymmetry that is nearly absent for $\Delta\lambda_{\mathrm{FWHM}} = 16\,\mathrm{nm}$, but grows gradually as the spectrum widens and appears maximal for $\Delta\lambda_{\mathrm{FWHM}} = 52\,\mathrm{nm}$. Simultaneously, the spectral maximum progressively shifts toward longer wavelengths as the spectrum widens. In the case of the widest spectrum, the 3 dB bandwidth extends up to 1600 nm. This behavior is due to Raman self-frequency shift (SFS), which affects the intracavity pulse evolution for the higher-power pulses. Note finally that the spectra measured at Outputs 1 and 2 are quite similar, except that the latter is slightly red-shifted with respect to the former (compare dashed and dotted curves in Fig. 3 for $\Delta\lambda_{\mathrm{FWHM}} = 24\,\mathrm{nm}$), due to the Raman SFS taking place in the 100 m long NOLM loop.

The noncollinear autocorrelation of the pulses was also measured for different positions of the HWR where mode locking was observed. The traces measured at Output 1 are presented in Fig. 4. For all positions of the HWR where mode locking is found, the autocorrelation presents a narrow subps peak riding a wide pedestal that extends beyond the 200 ps measurement window. Invariably, the ratio between the peak intensity and the pedestal level is ~2. Figure 4 also shows that the temporal properties of the pulses depend substantially on the HWR position. As the spectral bandwidth increases, the durations of both the pedestal and the central peak of the autocorrelation trace decrease. The shorter pedestal (corresponding to 52 nm bandwidth) presents a full width at half maximum (FWHM) duration of ~200 ps. The maximal FWHM pedestal duration (corresponding to 16 nm bandwidth) is estimated to be ~3 times larger, although a precise measurement is not possible due to the limited scanning range of the autocorrelator. Finally, the FWHM duration of the central peak varies between ~140 and ~270 fs.

The pulses were also measured using a 2 GHz photodetector and a sampling oscilloscope. Figure 5 presents the traces obtained for different positions of the HWR. In spite of the limited bandwidth of the detection setup, a dependence of the waveform duration with the HWR position can be appreciated, which is consistent with the behavior of the pedestal

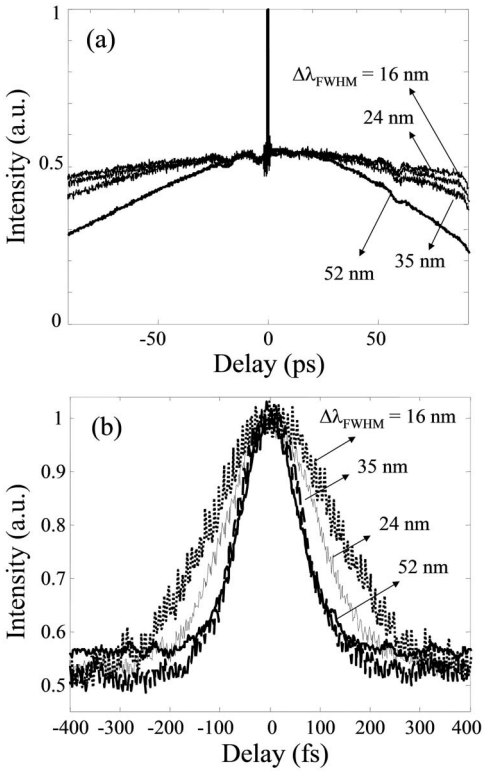

Fig. 4. Autocorrelation traces for different positions of the HWR, measured with two different time scales. Values of 3 dB bandwidth are indicated as curve labels.

of the autocorrelation trace in Fig. 4(a). The energy of the pulses at Output 1 was estimated to be ~1.4 nJ, and is quite independent of the HWR position, as the measured variation is only of ~8% when the HWR position is varied over the whole range of mode locking. The energy variation is more significant at Output 2, due to variation of the NOLM transmission. At Output 1, pulses with 1.4 nJ energy at 1.6 MHz repetition rate correspond to an average power of 2.2 mW, a value that is consistent with the measured output power of 4 mW, and that shows that the energy of the output signal is mainly contained in the pulses.

The variation of the NOLM switching power with the HWR angle when input polarization is linear was

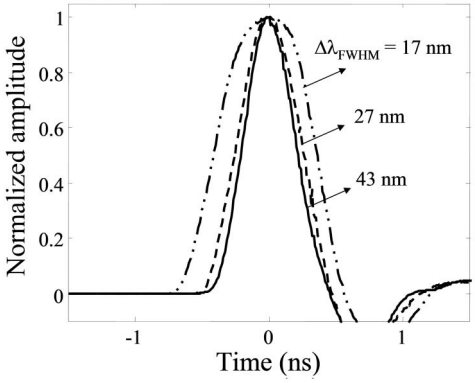

Fig. 5. Sampling oscilloscope traces of the pulses detected at Output 1, for different positions of the HWR. The values of the 3 dB bandwidth are included in the figure.

demonstrated in [23]. In the present work, the NOLM switching power was not directly measured; however it can be estimated from the measured pulse characteristics, if we assume that, in the regime of mode-locking operation, their peak power at the NOLM input roughly matches the NOLM switching power. Considering that the pulse energy at the NOLM input is nine times the value measured at Output 1, and estimating the pulse duration in each case from the autocorrelation traces, one can get an estimate of the pulse peak power, assuming a Gaussian profile. Finally, it should be considered that the pulses are actually packets of a large number of ultrashort pulses with varying amplitudes, whose peak power reaches up to four times the amplitude of their envelope [29]. The values of switching power obtained from these considerations are 103, 155, 225, and 335 W, corresponding to signal bandwidth values of 16, 24, 35, and 52 nm, respectively. These estimates are quite realistic, in particular the first value closely matches the minimal switching power value of the 100 m long NOLM calculated in section 2.

4. Numerical Study and Discussion

The figure-eight laser was modeled and its operation was analyzed numerically. The scheme considered (Fig. 6) is very similar to the experimental setup of Fig. 1. The length of the NOLM (100 m) and of the EDF (4 m) are chosen equal to the experiment, and a piece of 16 m of fiber at the NOLM input accounts for the pigtails of the components inserted in the ring section of Fig. 1 (couplers, isolator, polarizer, wave plates). The values of dispersion (17 ps/nm/km for standard fiber and −70 ps/nm/km for EDF) and nonlinear coefficient γ (1.5 /W/km) were also chosen to match the experimental conditions. The QWR angle is chosen to ensure low-power NOLM transmission ≈ 0.1 with a positive slope at $P_{\text{in}} = 0$. The polarization at the NOLM input is linear, and its angle ψ with respect to the QWR, which determines the NOLM switching power, is one of the simulation parameters. Propagation in the fiber sections of the laser is modeled using a pair of extended nonlinear Schrödinger equations, which are integrated using the split-step Fourier method. In the circular polarization basis $[C^+, C^-]$, these equations write as [30]

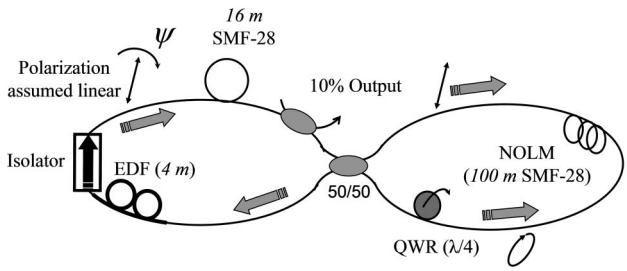

Fig. 6. Setup used for numerical simulations.

$$
\begin{aligned}
\frac{\partial C^+}{\partial z} &= -\frac{\Delta\beta_1}{2}\frac{\partial C^+}{\partial t} - j\frac{\beta_2}{2}\frac{\partial^2 C^+}{\partial t^2} \\
&\quad + j\frac{2}{3}\gamma(|C^+|^2 + 2|C^-|^2)C^+ \\
&\quad - j\gamma T_R\left[\frac{1}{2}\frac{\partial}{\partial t}(|C^+|^2 + |C^-|^2)C^+\right. \\
&\quad \left. + \frac{\partial}{\partial t}(\mathrm{Re}(C^+C^{-*}))C^-\right] + \frac{g}{2}C^+ + \frac{1}{L_a\Omega_a^2}\frac{\partial^2 C^+}{\partial t^2}; \\
\frac{\partial C^-}{\partial z} &= +\frac{\Delta\beta_1}{2}\frac{\partial C^-}{\partial t} - j\frac{\beta_2}{2}\frac{\partial^2 C^-}{\partial t^2} + j\frac{2}{3}\gamma(|C^-|^2 + 2|C^+|^2)C^- \\
&\quad - j\gamma T_R\left[\frac{1}{2}\frac{\partial}{\partial t}(|C^+|^2 + |C^-|^2)C^-\right. \\
&\quad \left. + \frac{\partial}{\partial t}(\mathrm{Re}(C^+C^{-*}))C^+\right] + \frac{g}{2}C^- + \frac{1}{L_a\Omega_a^2}\frac{\partial^2 C^-}{\partial t^2}.
\end{aligned}
\tag{1}
$$

The first right-hand terms of Eq. (1) take into account the group velocity mismatch between the C^+ and C^- components, the second and third terms are dispersive and Kerr nonlinear terms, respectively, and the fourth terms account for Raman SFS [11]. Finally, the last two terms stand for gain and gain dispersion, and are considered for integration over the doped fiber section only. The coefficient $\Delta\beta_1 = \beta_1^+ - \beta_1^- = 1/v_g^+ - 1/v_g^-$ is the inverse group velocity mismatch, β_2 is the second-order dispersion (expressed in ps^2/km), T_R is the Raman delay, L_a is the amplifier length, Ω_a its bandwidth in Hz (half-width at $1/e$ from the maximum) and g is the gain per unit length. Here g is assumed to be constant along the doped fiber, and saturates on the pulse energy E_p as

$$
g(E_p) = \frac{g_0}{1 + E_p/E_{\text{sat}}}, \tag{2}
$$

where g_0 is the small-signal gain and E_{sat} is the saturation energy. The value of g_0 was chosen large enough to ensure that low-power gain exceeds the low-power cavity losses and the value of E_{sat} (.15 nJ) was chosen in order to obtain results comparable with the experiment, in particular in terms of pulse energy, yet keeping the computational time within reasonable limits. The FWHM gain bandwidth was set to 50 nm, and the Raman parameter $T_R = 3$ fs. Finally, the group velocity mismatch was calculated on the basis of a twist of 5 turns/m (yielding a delay of ∼2.5 fs/m between C^+ and C^-).

Taking a small-amplitude Gaussian noise as the initial signal, integration is performed over successive cycles. The formation of noiselike pulses was observed for a limited range of values of the NOLM input polarization angle ψ, extending over $0.85\pi/2$ rad around $\pi/4$. For the NOLM parameters used in these simulations, the switching power varies over this interval from a minimal value of ∼110 W for $\psi = \pi/4$ to ∼500 W for $\psi = 0.15\pi/4$ and $1.85\pi/4$. Even though a strict-sense convergence was not observed, a globally stable output waveform is

generally obtained after a limited number of integration cycles (~15–25). Although the exact shape of the waveform keeps changing after successive round trips, its global features, in particular its duration, energy and optical bandwidth, remain stable. Figure 7(a) shows output waveforms obtained for different values of ψ (and of NOLM switching power). They correspond to subns packets containing a large number of subps pulses with randomly varying intensities. More interestingly, one can observe that the total duration of the packet decreases (from ~100 to ~6 ps) and the peak power increases significantly as the switching power increases. The energy of the pulses lies in the range of 0.32–0.38 nJ and it thus roughly constant, and does not vary with ψ.

Figure 7(b) shows the optical spectra calculated for the same values of ψ as in Fig. 7(a), averaged over 10 pulses and seen through a 2 nm resolution filter. Wide and smooth spectra are obtained, which is consistent with the experimental results (Fig. 3). It has to be noted that averaging is critical to guarantee the smoothness of the spectrum; indeed, as observed earlier [13], the spectrum of an individual waveform presents a very spiky and irregular shape, which hardly compares with the experiment. Although the bandwidths of the simulated spectra are smaller than the experimental values, spectral widening is observed as the NOLM critical power is increased, in agreement with the experiment. The FWHM bandwidth varies between 8 and 21 nm. Finally, spectral asymmetry appears as a consequence of Raman SFS, like in the experiment. Note that even though spectral widening is enhanced by the Raman SFS, considering this effect is not necessary to obtain the noiselike pulse regime, as it was verified numerically by dropping the fourth right-hand terms in Eq. (1).

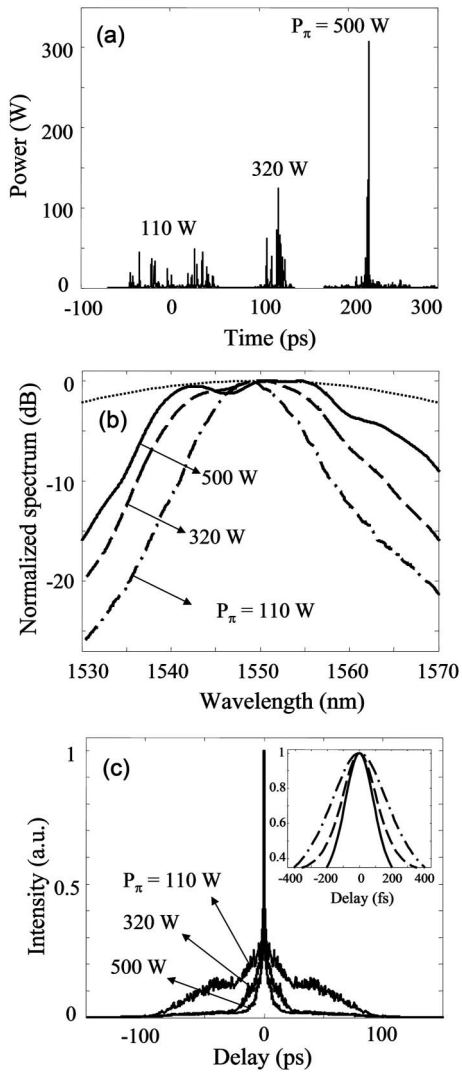

Fig. 7. (a) pulse profiles, (b) optical spectra and (c) autocorrelation traces simulated for the NOLM switching power values of 110 W, 320 W and 500 W. The Gaussian spectrum of the amplifier used in the simulations is also shown in Fig. (b) (dotted).

Figure 7(c) presents the simulated autocorrelation traces averaged over 10 pulses, for the same values of ψ as previously. The shape is in quite good agreement with the experiment (Fig. 4), with a subps central peak riding a subns pedestal. The extension of the pedestal strongly varies with ψ, which is expected as the pedestal duration reflects the total duration of the waveform, and this behavior is also in agreement with the experiment. More interestingly, the inset in Fig. 7(c) shows that the duration of the coherence peak also decreases as the switching power is increased, from ~400 fs to ~200 fs. Considering that the duration of the central narrow peak reflects the average duration of the pulses in the packet, this means that the durations of these pulses globally decrease as the switching power increases, although these durations remain largely variable in the packet. It has to be noted that the ratio between central peak power and pedestal level in the simulated autocorrelation is ~3, unlike the experiment. We noted however that this value is variable along the cavity, and is mostly related to the values of dispersion of the different sections of fiber. For example, if the autocorrelation is calculated at the doped fiber output, the ratio is as small as 1.5.

Although all publications dealing with noiselike pulses present similar experimental results (in particular an autocorrelation with a narrow spike riding a wide and smooth pedestal, and a wide and smooth optical spectrum), different physical mechanisms are invoked, all successfully reproducing these results numerically. One reason for this convergence is related to the ambiguity of the autocorrelation function, which reaches its paroxysm in the case of pulses presenting a complex inner structure: quite independently of the details of the rapid inner pulse oscillations, roughly the same autocorrelation is obtained, taking the form of a narrow coherence spike riding the autocorrelation function of the slowly varying pulse envelope [31]. Moreover, considering the wide variability of the details of the subpulses after successive round trips, and the short and constant duration of the coherence spike, it is easy to understand that a wide spectrum, which has been cleaned

out from all noisy fluctuations through strong averaging, is invariably obtained.

Considering the arguments discussed above, autocorrelation and spectral measurements, and their coincidence with their simulated counterparts are not very helpful to reveal the mechanism of noiselike pulse formation. In spite of this, our numerical results give elements to discuss pulse formation in the figure-eight laser, in particular considering the mechanisms proposed previously for fiber ring lasers. In [6], the large and nonuniform birefringence of the laser cavity is the key element that leads to noiselike pulse formation. In the present setup, birefringence is essentially induced by twist, so that it is circular and uniform, and its value, estimated to be $\Delta n \approx 9 \times 10^{-7}$, is rather small. Hence, a dominant effect of strong nonuniform birefringence in pulse formation is not likely. To verify this, we repeated the simulations with the same parameters as previously, except that the first right-hand terms in Eq. (1), which stand for twist-induced group velocity mismatch between polarization components, were dropped. No significant difference was observed in comparison with the previous results, in particular in terms of pulse duration, spectral width and shape.

In [10], pulse formation was related to the pulse collapse effect. In the presence of gain and positive saturable absorber feedback, under certain conditions ultrashort pulse evolution is characterized by an explosive growth of peak power and reduction of duration (with consequent increase in bandwidth). If the pulse is not stabilized by a relatively low switching point of the nonlinear switching element, this evolution is eventually stopped anyway at some point, resulting in the destruction of the pulse, whose noisy remnants serve as the seeds of subsequent pulse growth and destruction. A large number of such pulses at different stages of this cyclic evolution form the observed bunches. The stopping of the explosive pulse growth and pulse destruction can be attributed to high-order nonlinear switching terms [13], or to gain dispersion when the pulses spectral width becomes comparable with gain bandwidth [11]. Even though the latter mechanism may be at play in the experiment, where the signal bandwidth (up to 52 nm) is comparable to the gain bandwidth, it is not necessary, according to numerical results, for the formation of noiselike pulses, as it appears in Fig. 7(b) where the pulse spectra are in all cases substantially narrower than the gain bandwidth. Moreover, according to both experimental and numerical results, the longest bunches, which contain the largest number of pulses, and thus for which in one sense the "noiselike" nature is most evident, correspond to the narrowest spectrum, less likely to be affected by gain bandwidth limitation.

The importance of the switching power value for determining the regime of mode locking has already been recognized [10]: if the switching point is low enough, the pulse peak power is stabilized and the laser operates in a conventional, solitonlike mode of operation. If now the switching is too high, a single pulse is unstable and evolves toward a noiselike pulse before it can reach the switching point. In a normal-dispersion cavity, the dependence of the noiselike pulse spectrum on the adjustment of switching power was evidenced, and pulse formation was attributed to peak power clamping to the switching point causing dispersive wave growth [12]. In this Paper, we show both experimentally and numerically that the value of switching power is critical in determining the temporal and spectral properties of the noiselike pulses, and therefore that controlling this value constitutes a convenient way of tuning the pulse characteristics. Indeed, for a given available energy, a low switching power limits the growth of the pulse peak power, which favors the formation of a large number of pulses with relatively low peak powers and correspondingly large durations (and narrow spectrum). If now the switching power is large, the solitons are allowed to grow to higher peak power values, associated with shorter durations; besides, as the energy of the individual pulses is higher, their number is smaller and they are packed into a shorter bunch. In spite of this influence however, the NOLM switch does not appear as the sole responsible for the onset of the noiselike pulse mode of operation. Indeed, for the laser parameters used in this Paper, conventional single-pulse operation was never observed, neither in the experiment nor in simulations, in particular when the switching power was decreased to its minimum value to prevent pulse collapse [10] or, inversely, when it was raised to an arbitrarily high value to prevent either peak power clamping that would favor the growth of dispersive waves [12], or of NOLM overdriving that would tend to split an individual pulse into several pulses. In both experiment and numerical simulations, beyond a certain range of the NOLM input polarization orientation, mode locking is lost. Hence it appears that the value of the switching point does not offer a complete explanation for the noiselike pulse operation of our laser, so that an additional ingredient is required, which may involve pulse collapse [10] or the instability of ultrashort pulses under certain laser cavity conditions [13].

5. Conclusion

In this work we study experimentally and numerically a figure-eight laser scheme including a polarization-imbalanced NOLM with linear input polarization. Thanks to the use of a HWR, the angle of linear polarization at the NOLM input can be adjusted, which allows controlling the NOLM switching power. For proper adjustments of the QWR inserted in the loop (which determines the NOLM low-power transmission) and of the HWR, the laser generates a stable pulse train at the fundamental frequency of 1.6 MHz. The noiselike nature of the pulses (actually subns bunches of many subps pulses with randomly varying amplitude and duration) is evidenced by the double-scaled structure of the autocorrelation and the large bandwidth and smoothness of the optical

spectrum. Although mode locking is not self-starting, stable pulsed operation is obtained over a range of the HWR orientation. The variation of the HWR orientation over that range allows adjusting the spectral and temporal properties of the generated pulses. As the HWR is rotated, the pulse spectral bandwidth grows from 16 to 52 nm, and the onset of Raman SFS progressively shifts the spectrum toward larger wavelengths. Simultaneously, the duration of the bunch as well as the inner subps pulses reduce, whereas peak power evolves inversely. The output pulse energy (~1.4 nJ) is quite independent of the HWR adjustment. Numerical simulations are in good qualitative agreement with experimental results, and confirm the possibility to adjust the pulse characteristics through switching power adjustment. They also show that, in spite of the critical role of the NOLM switching point to define the pulse parameters, peak power clamping or NOLM overdriving does not yield a complete picture of the noiselike pulse regime in this laser. Such sources are attractive for several applications, for example in metrology, when low temporal coherence is required, or for seeding supercontinuum generation, as they combine the advantages of high energy of nanosecond pulses with the wide spectrum proper to femtosecond pulses.

O. Pottiez was supported by Consejo Nacional de Ciencia y Tecnología (CONACyT) grant 130 681.

References

1. V. J. Matsas, D. J. Richardson, T. P. Newson, and D. N. Payne, "Characterization of a self-starting, passively mode-locked fiber ring laser that exploits nonlinear polarization evolution," Opt. Lett. **18**, 358–360 (1993).
2. I. N. Duling III, "All-fiber ring soliton laser mode locked with a nonlinear mirror," Opt. Lett. **16**, 539–541 (1991).
3. N. J. Doran and D. Wood, "Nonlinear optical loop mirror," Opt. Lett. **13**, 56–58 (1988).
4. M. E. Fermann, F. Haberl, and M. Hofer, "Nonlinear amplifying loop mirror," Opt. Lett. **15**, 752–754 (1990).
5. F. Ö. Ilday, F. W. Wise, and T. Sosnowski, "High-energy femtosecond stretched-pulse fiber laser with a nonlinear optical loop mirror," Opt. Lett. **27**, 1531–1533 (2002).
6. M. Horowitz, Y. Barad, and Y. Silberberg, "Noiselike pulses with a broadband spectrum generated from an erbium-doped fiber laser," Opt. Lett. **22**, 799–801 (1997).
7. M. Horowitz and Y. Silberberg, "Control of noiselike pulse generation in erbium-doped fiber lasers," IEEE Photon. Technol. Lett. **10**, 1389–1391 (1998).
8. J. U. Kang, "Broadband quasi-stationary pulses in mode-locked fiber ring laser," Opt. Commun. **182**, 433–436 (2000).
9. Y. Takushima, K. Yasunaka, Y. Ozeki, and K. Kikuchi, "87 nm bandwidth noise-like pulse generation from erbium-doped fibre laser," Electron. Lett. **41**, 399–400 (2005).
10. D. Y. Tang, L. M. Zhao, and B. Zhao, "Soliton collapse and bunched noise-like pulse generation in a passively mode-locked fiber ring laser," Opt. Express **13**, 2289–2294 (2005).
11. L. M. Zhao and D. Y. Tang, "Generation of 15 nJ bunched noise-like pulses with 93 nm bandwidth in an erbium doped fiber ring laser," Appl. Phys. B **83**, 553–557 (2006).
12. L. M. Zhao, D. Y. Tang, and J. Wu, "Noise-like pulse in a gain-guided soliton fiber laser," Opt. Express **15**, 2145–2150 (2007).
13. S. Kobtsev, S. Kukarin, S. Smirnov, S. Turitsyn, and A. Latkin, "Generation of double-scale femto/pico-second optical lumps in mode-locked fiber lasers," Opt. Express **17**, 20707–20713 (2009).
14. M. L. Dennis, M. A. Putnam, J. U. Kang, T.-E. Tsai, I. N. Duling III, and E. J. Friebele, "Grating sensor array demodulation by use of a passively mode-locked fiber laser," Opt. Lett. **22**, 1362–1364 (1997).
15. K. Tamura, E. P. Ippen, H. A. Haus, and L. E. Nelson, "77 fs pulse generation from a stretched-pulse mode-locked all-fiber ring laser," Opt. Lett. **18**, 1080–1082 (1993).
16. L. E. Nelson, S. B. Fleischer, G. Lenz, and E. P. Ippen, "Efficient frequency doubling of a femtosecond fiber laser," Opt. Lett. **21**, 1759–1761 (1996).
17. J. R. Buckley, F. W. Wise, F. Ö. Ilday, and T. Sosnowski, "Femtosecond fiber lasers with pulse energies above 10 nJ," Opt. Lett. **30**, 1888–1890 (2005).
18. A. I. Chernykh and S. K. Turitsyn, "Soliton and collapse regimes of pulse generation in passively mode locking laser systems," Opt. Lett. **20**, 398–400 (1995).
19. M. Attygalle, A. Nirmalathas, and H. F. Liu, "Novel technique for reduction of amplitude modulation of pulse trains generated by subharmonic synchronous mode-locked laser," IEEE Photon. Technol. Lett. **14**, 543–545 (2002).
20. W. S. Wong, S. Namiki, M. Margalit, H. A. Haus, and E. P. Ippen, "Self-switching of optical pulses in dispersion-imbalanced nonlinear loop mirrors," Opt. Lett. **22**, 1150–1152 (1997).
21. E. A. Kuzin, N. Korneev, J. W. Haus, and B. Ibarra-Escamilla, "Theory of nonlinear loop mirrors with twisted low-birefringence fiber," J. Opt. Soc. Am. B **18**, 919–925 (2001).
22. O. Pottiez, E. A. Kuzin, B. Ibarra-Escamilla, and F. Mendez-Martinez, "Theoretical investigation of the NOLM with highly twisted fibre and a $\lambda/4$ birefringence bias," Opt. Commun. **254**, 152–167 (2005).
23. B. Ibarra-Escamilla, E. A. Kuzin, P. Zaca-Moran, R. Grajales-Coutiño, F. Mendez-Martinez, O. Pottiez, R. Rojas-Laguna, and J. W. Haus, "Experimental investigation of the nonlinear optical loop mirror with twisted fiber and birefringence bias," Opt. Express **13**, 10760–10767 (2005).
24. E. A. Kuzin, B. Ibarra-Escamilla, D. E. Garcia-Gomez, and J. W. Haus, "Fiber laser mode locked by a Sagnac interferometer with nonlinear polarization rotation," Opt. Lett. **26**, 1559–1561 (2001).
25. B. Ibarra-Escamilla, O. Pottiez, E. A. Kuzin, J. W. Haus, R. Grajales-Coutiño, and P. Zaca-Moran, "Experimental investigation of self-starting operation in a F8L based on a symmetrical NOLM," Opt. Commun. **281**, 1226–1232 (2008).
26. B. Ibarra-Escamilla, O. Pottiez, J. W. Haus, E. A. Kuzin, M. Bello-Jimenez, and A. Flores-Rosas, "Wavelength-tunable picosecond pulses from a passively mode-locked figure-eight Erbium-doped fiber laser with a Sagnac fiber filter," J. Eur. Opt. Soc. **3**, 08036 (2008).
27. T. Tanemura and K. Kikuchi, "Circular birefringence fiber for nonlinear optical signal processing," J. Lightwave Technol. **24**, 4108–4119 (2006).
28. O. Pottiez, B. Ibarra-Escamilla, and E. A. Kuzin, "Large signal-to-noise-ratio enhancement of ultrashort pulsed optical signals using a power-symmetric Nonlinear Optical Loop Mirror with output polarization selection," Opt. Fiber Technol. **15**, 172–180 (2009).
29. V. E. Zacharov and A. B. Shabat, "Exact theory of two-dimentional self-focusing and one-dimentional self modulation of waves in nonlinear media," Sov. Phys. JETP **61**, 62–69 (1972).
30. G. P. Agrawal, *Nonlinear Fiber Optics* (Academic Press, 1995).
31. R. Trebino, *Frequency Resolved Optical Gating: the Measurement of Ultrashort Optical Pulses* (Kluwer Academic Publishers, 2000).